Earth and Planetary Science Letters 410 (2015) 117–127

Contents lists available at ScienceDirect

Earth and Planetary Science Letters

www.elsevier.com/locate/epsl

Slow and delayed deformation and uplift of the outermost subduction prism following ETS and seismogenic slip events beneath Nicoya Peninsula, Costa Rica

Earl E. Davis [a,*], Heinrich Villinger [b], Tianhaozhe Sun [a,c]

[a] Pacific Geoscience Centre, Geological Survey of Canada, 9860 W. Saanich Rd., Sidney, BC, V8L 4B2, Canada
[b] FB Geowissenschaften, University of Bremen, Postfach 330 440, D-28334, Bremen, Germany
[c] School of Earth and Ocean Science, University of Victoria, PO Box 1700, Victoria, BC, V8W 2Y2, Canada

ARTICLE INFO

Article history:
Received 31 May 2014
Received in revised form 12 November 2014
Accepted 15 November 2014
Available online 5 December 2014
Editor: P. Shearer

Keywords:
subduction zones
aseismic slip
episodic tremor and slip
subduction prism deformation
tsunami generation
borehole monitoring

ABSTRACT

Two ODP CORK (Ocean Drilling Program circulation obviation retrofit kit) borehole hydrologic observatory sites deployed in 2002 at the toe of the subduction prism off Nicoya Peninsula, Costa Rica were visited in December 2013. The five years of seafloor and formation fluid pressure data collected since the previous visit include clear signals associated with an episodic tremor and slip (ETS) event off the coast of Nicoya Peninsula in 2009, and a Mw 7.6 subduction thrust earthquake beneath the Peninsula in 2012. Formation pressure anomalies associated with the ETS event are similar to ones observed following ETS events observed previously here, as well as ones following very low frequency earthquake swarms within the Nankai accretionary prism off southwestern Japan. Positive and negative impulsive transients in the hanging wall and foot wall of the subduction thrust, respectively, suggest contractional and dilatational strain generated by local slip propagating up the thrust fault beneath the outermost prism. In the case of the 2009 event, the transients occurred roughly two weeks after the initiation of slip observed at GPS sites along the adjacent coast. At the same time, a decrease in seafloor pressure at the prism site relative to the subducting plate was observed, indicating concurrent uplift of the prism of 1.2 cm. Other events at the prism toe following ETS events closer to the coast are seen in 2006, 2007, 2008, 2010, and 2011. The time between the initiation of ETS slip constrained by GPS and the onset of the prism toe transients suggest up-dip "rupture" propagation along the seaward part of the subduction thrust at rates of a few km/day. In the case of the 2009 event, the slip at the prism toe (*c.* 11 cm), estimated from the 1.2 cm uplift and the local dip on the decollement (6°), is roughly a factor of 5 greater than the slip further landward estimated from GPS data by Dixon et al. (in press). In other cases, slip at the toe is less or unresolvable. Similar uplift and formation fluid pressure transients occurred two days after the 2012 Nicoya thrust earthquake, then episodically (unrelated to aftershocks) every 1–3 weeks over the next few months. Slip rates at the prism toe, estimated from the magnitude and duration of these and ETS-related uplift events, are roughly 5 cm/day. Such rates are much too slow for tsunamigenesis or seismogenesis. Total slip of the outermost prism after the 2012 earthquake, determined from the uplift accumulated until the end of the observation period and the estimated local fault dip, is roughly 75 cm, a significant fraction of the seismogenic slip of the Mw 7.6 earthquake itself (a maximum of over 3 m). Negative steps in formation pressure are observed at both the prism and subducting plate sites simultaneous with the 2012 thrust earthquake. The sign of these steps is inconsistent with the contractional deformation predicted by an elastic fault-dislocation model with slip limited to the seismogenic zone. Highly compliant (low shear modulus) sediment below the decollement, or very low-stress deformation along splay faults, may be responsible for the co-seismic dilatation observed in the outermost prism and incoming plate.

© 2014 Elsevier B.V. All rights reserved.

* Corresponding author.
E-mail address: edavis@nrcan.gc.ca (E.E. Davis).

http://dx.doi.org/10.1016/j.epsl.2014.11.015
0012-821X/© 2014 Elsevier B.V. All rights reserved.

1. Introduction

Most subduction seismogenic zones lie beneath continental shelves and slopes, quite often with the landward limit of slip located near coastlines and the seaward limit well offshore, whereas most seismic and geodynamic observations are made on land. This inherently limits the confidence with which determinations of coseismic and post-seismic slips can be made. Exceptions include locations like Costa Rica and Sumatra, where islands or peninsulas allow observations to be distributed at least partially over areas of seismogenic rupture, and Japan, where seafloor geodetic observatories have been recently established. Observations made at the time of earthquakes at these locations have provided new and valuable insights into the range of behavior of subduction thrusts, leading to great improvements in the understanding of seismogenic and tsunamigenic rupture (Hill et al., 2012; Hsu et al., 2006; Kido et al., 2011; Iinuma et al., 2012; Maeda et al., 2011; Japan Coast Guard and Tohoku University, 2013; Yue et al., 2013; Sun et al., 2014).

New insights have also been gained through various observations of deformation and associated non-volcanic tremor and low-frequency, low-stress-drop earthquakes swarms within and up dip of the seismogenic zone in interseismic periods (Obara and Ito, 2005; Ito and Obara, 2006; Hirose et al., 2010; Walter et al., 2011, 2013; Outerbridge et al., 2010; Jiang et al., 2012). These observations suggest that subduction thrust interfaces can be highly heterogeneous, with seismogenic patches surrounded by areas hosting deformation between times of major earthquakes (e.g., Davis et al., 2013; Protti et al., 2013; Dixon et al., in press). Episodes of deformation and anomalous seismic activity have in many cases been found to be frequent (event intervals of months to years) relative to the recurrence period of major earthquakes (tens to hundreds of years).

In this paper we present data gathered recently from two CORK borehole observatories off the Nicoya Peninsula, Costa Rica, established in 2002 during ODP Leg 205 to study the hydrogeology and deformation associated with subduction (Morris et al., 2003; Jannasch et al., 2003). Data and fluid samples collected prior to the recording period reported here have revealed a link between deformation observed deep along the plate interface (e.g., Protti et al., 2004; Outerbridge et al., 2010) and deformation at the prism toe borehole and seafloor observatory sites (Davis and Villinger, 2006; Labonte et al., 2009; Solomon et al., 2009; Davis et al., 2011). On the basis of these observations, it was inferred that episodic slip initiated beneath Nicoya Peninsula can propagate up dip all the way to the prism toe at rates averaging some 10 km per day (Davis and Villinger, 2006; Davis et al., 2011). Seafloor and formation pressure data gathered most recently from the two borehole sites span from February 2009 to December 2013, and include signals associated with a slip propagation event following an episodic tremor and slip (ETS) episode in mid-2009, as well as with a magnitude Mw 7.6 earthquake on the subduction plate interface beneath the coast of Nicoya Peninsula in September 2012. On the basis of tremor locations (S. Schwartz, pers. comm., 2014) and an inversion of GPS observations (Dixon et al., in press), the ETS event was estimated to be centered roughly 35 km offshore, roughly mid-way between the borehole observatory sites and the coast. In the case of the 2012 earthquake, the primary seismogenic slip estimated from seismic and GPS observations on the Nicoya Peninsula (Yue et al., 2013) was located beneath Nicoya Peninsula, with some slip extending roughly 40 km off the coast, i.e., roughly 30 km landward of the toe of the subduction prism (the seaward limit of the plate interface located along the inner Middle America Trench) (Fig. 1a). No significant tsunami was generated by this event.

2. Details of the CORK borehole observatories

Complete descriptions of the CORKs installed at these sites and the local structure and lithology have been published previously (Morris et al., 2003; Jannasch et al., 2003; Davis and Villinger, 2006), so only a brief summary is provided here. Hole 1253A was drilled into oceanic basement just seaward (*c.* 175 m) of the toe of the subduction prism (Fig. 1b) through 400 m of hemipelagic and pelagic sediment, a 31-m-thick gabbroic sill, 30 m of sediments underlying the sill, and an additional 140 m of igneous rocks that are probably part of uppermost extrusive basement. The primary objective for monitoring at this site was to document the average formation state in order to constrain the role of basement in creating a path for fluid flow from the base of the accretionary complex, and hence in possibly influencing the average pressure state and mechanical properties of the subduction complex further landward. For the purposes of the current investigation, the hole provides a view of fluid pressure, and hence volumetric strain, in the footwall of the seaward-most part of the subduction-zone thrust fault, although this view is limited by the high permeability of the igneous section and the speed at which strain-induced pressure anomalies dissipate. Hole 1255A, located 920 m landward of Hole 1253A, was drilled into the toe of the subduction prism to a total depth of 153 m below the seafloor (mbsf), just beyond the base of the subduction decollement at 144 mbsf. Monitoring at this site was intended to provide constraints on the pressure state in the decollement and in the hanging wall of the thrust, and to allow possible pressure transients to be documented. The sites lie roughly 70 km from the Nicoya Peninsula coast.

Each CORK includes 1) mechanical seals at the seafloor (between the primary $10\frac{3}{4}''$ diameter formation casing and the secondary $4\frac{1}{2}''$ diameter CORK-II casing) and at the bottom of the CORK-II casing (where a removable fluid sampling instrument is situated), and 2) a single hydraulically inflated packer at an intermediate position in the formation. These seals isolate formation intervals that span from the bottom of each hole to the packers, and from the packer to the base of the primary cemented borehole casing. Formation pressures in these intervals are transmitted to sensors at the wellheads via thick-walled stainless steel hydraulic lines that are terminated at depth in wire-wrapped filter screens. The upper screens are devoted to pressure monitoring only, and are 2.5 cm in diameter and 1.5 m long. The lower screens serve for pressure monitoring as well as formation-fluid sampling; they wrap around the full circumference of the osmosampler instrument, and are 7.6 m long. If the formation collapses around the screens (as is likely in the sedimentary sections), pressures will be representative of local conditions at each screen; if the hole remains largely intact (as probably the case in the igneous units), pressures will represent an average state (weighted by hydraulic diffusivity) over the full length of the isolated sections.

At Site 1253, the upper interval isolated for pressure monitoring spans a mixed lithologic section comprising a gabbroic sill from the base of the $10\frac{3}{4}''$ casing at 413 mbsf to 431 mbsf, a high-porosity (65–70%) sedimentary unit from 431 to 461 mbsf, and igneous rocks from 461 mbsf to the packer at 473 mbsf (Morris et al., 2003). The lower interval from the packer to the bottom of the hole at 600 mbsf penetrates igneous rocks with fractured intervals and/or possibly minor sediment interbeds. The upper and lower screens are centered at 453 and 500 mbsf, respectively. The $10\frac{3}{4}''$ casing is grouted into a massive interval of the upper sill, and the packer is seated in the deeper igneous section at a level that is inferred to be free of fractures on the basis of logging data and recovered cores.

At Site 1255, the upper interval from the base of the casing at 117 mbsf to the packer at 129 mbsf intersects *c.* 55% porosity sediment of the overthrust subduction prism toe above the

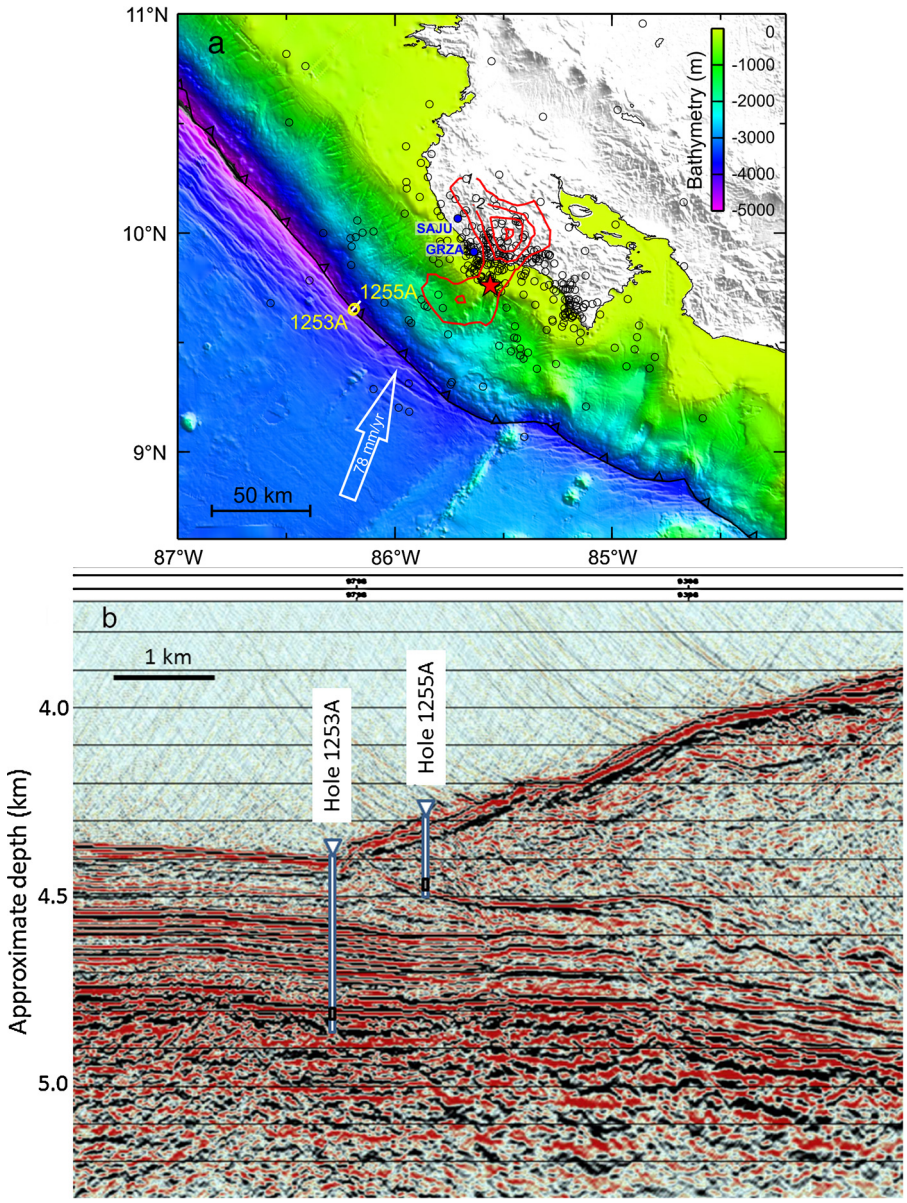

Fig. 1. Map showing the Nicoya Peninsula of Costa Rica, offshore bathymetry, CORK site locations (yellow labels), coastal GPS observatory site locations (blue labels, Jiang et al., 2012), and the epicenter (red star), estimated slip distribution (red contours in m), and aftershocks (black open circles) of the 2012 Mw 7.6 earthquake (from Yue et al., 2013; J. Walter, pers. comm., 2014) (a). Cross-strike seismic reflection profile through the CORK observatory sites, with pressure monitoring screen positions (black rectangles filled grey) shown schematically in context of the structure of the incoming oceanic plate and outer subduction prism (b). Location of the seismic line is shown by the short yellow line in (a). (For interpretation of the references to color in this figure legend, the reader is referred to the web version of this article.)

decollement zone (Morris et al., 2003). The lower interval, from 129 to 153 mbsf, intersects the decollement zone, the base of which lies at 144 mbsf, and the uppermost part of the underthrust sediment section, where porosity is typically close to 70%. In this hole, collapse of the formation around both screens is likely; the upper and lower screens are centered at 127 and 140 mbsf and span depths from 126.2 to 127.7 and 136.4 to 144.0 mbsf, respectively.

Absolute pressures at both sites are measured at the seafloor and in each of the two formation lines with model 8B-7000-2 sensors manufactured by Paroscientific, Inc. A resolution of roughly 1 ppm of the full 7000 m range of the sensors is achieved, i.e., 0.07 kPa, or 7 mm of equivalent water head. Pressure values are recorded in the CORK data loggers (manufactured by Richard Brancker Research, Ltd., Canada) at an interval of 10 min. This programmable interval was chosen to allow the monitoring experiment to extend over a lifetime of *c.* 20 yr with the 175 A/h batteries installed, although shelf-life limitations may ultimately limit the realized operation time. Data are stored in an 8 MB RAM, and are retrieved via an RS-232 communications link which also allows the logging interval, pressure resolution, and other parameters to be revised. Resistance of a thermistor, mounted on the end cap of the pressure vessel, is also measured and logged at 1 h intervals to provide a continuous record of bottom-water temperature variations with sub-mK resolution (e.g., Thomson et al., 2010).

3. Overview of observations

3.1. Formation pressures

Formation pressure anomalies shown in Figs. 2–5 have had the effects of oceanographic loading removed by subtracting the pressure measured at the seafloor, scaled by the observed tidal loading efficiency, from the raw formation signal. Sensor drift, as

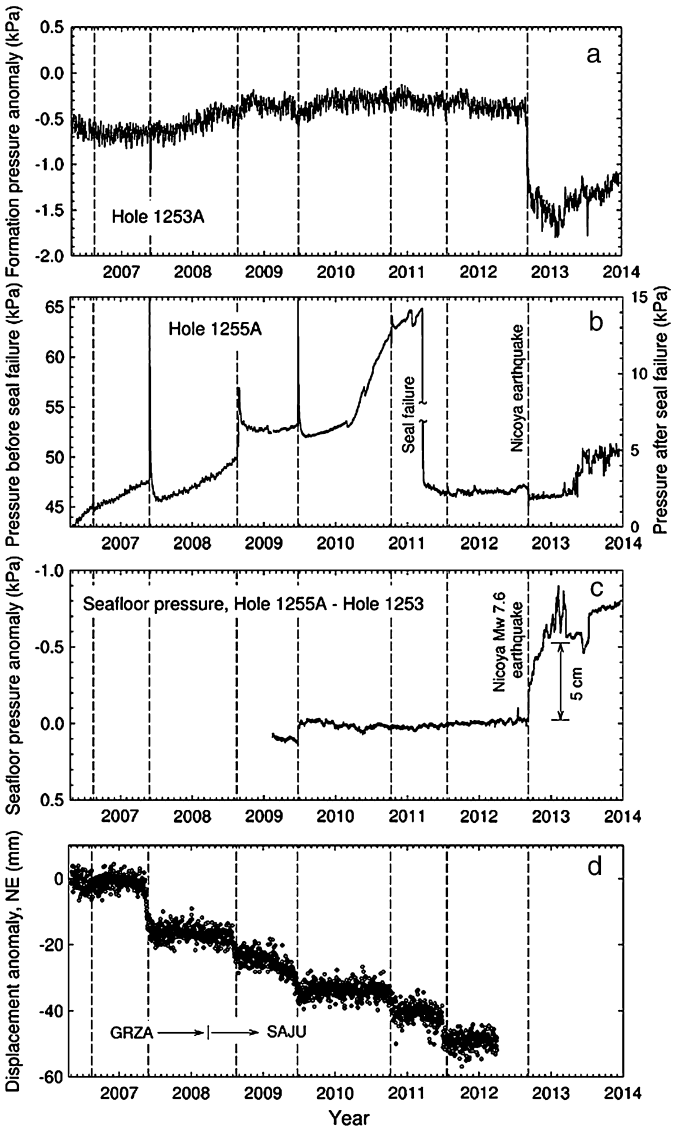

Fig. 2. Formation pressure data from Holes 1253A (a) and 1255A (b), with sensor drift removed using linear trends between hydrostatic checks at times of submersible visits, seafloor loading removed using observed tidal loading efficiencies, and residual tidal-frequency variations filtered with a 12.5-h averaging window. Formation tidal response relative to seafloor loading remains in phase, and with constant amplitudes at 0.58 and 0.93 at Holes 1253A and 1255A, respectively, until the loss of hydrologic integrity at Hole 1255A screen 2 in early 2011. At that time, average pressure fell to near-hydrostatic (note scale change), and formation tidal variations began to lag seafloor tidal loading variations. Seafloor pressure for the most recent recording interval is shown for Site 1255 using seafloor pressure at Site 1253 as a reference, after corrections were made for clock drift at each site (c). The site-to-site pressure difference was then filtered as in (a) and (b). Data shown in Figs. 3–5 were processed similarly. Seafloor pressure scaling here and in Figs. 3–5 is inverted to indicate equivalent uplift. Bottom panel (d) shows daily GPS observations from two coastal sites most proximate to the offshore borehole observatories (locations shown in Fig. 1; data from Jiang et al., 2012), with east and west components resolved in a direction perpendicular to the strike of the trench, and with trends based on data between slip events removed. ETS events seen at the coastal GPS sites are indicated by dashed lines at times defined by the onset of offshore CORK pressure transients. Other events observed at GPS sites further inland and to the southeast (Jiang et al., 2012) are not included.

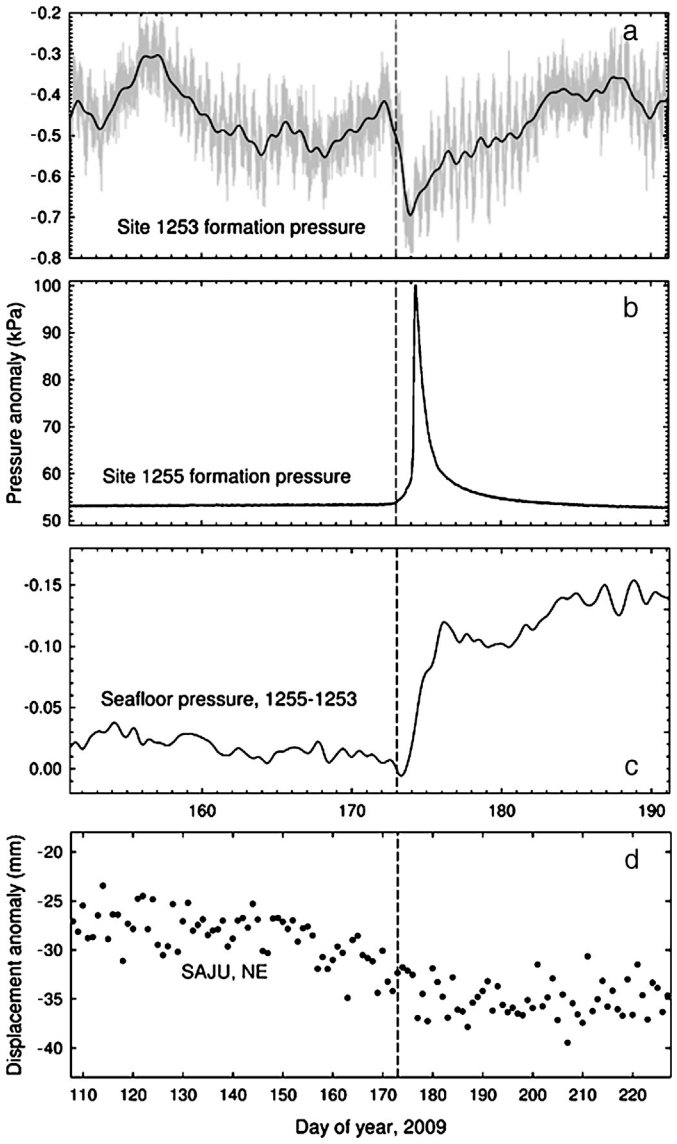

Fig. 3. Detailed views of non-hydrostatic formation pressure anomalies in Holes 1253A (a) and 1255A (b), seafloor pressure at Hole 1255A relative to Hole 1253A (c) with the depth difference removed, and daily GPS data at the time of the 2009 June ETS event (d). Data are shown unfiltered and tidally filtered in (a) unfiltered in (b), and filtered in (c) (see Fig. 2 caption for details). Dashed lines are shown at the time of initiation of pressure transients for reference. Note difference in time scales between (a–c) and (d).

determined by hydrostatic calibrations at the times of each visit, was also accounted for. Removal of the effects of oceanographic loading leads to formation pressure anomalies that are nearly free of loading effects, although there does remain a residual associated with earth tide, and possibly with hydrologic diffusion within the formation that can produce frequency-dependent phase differences between the seafloor loading and formation signals. To remove these residuals, a 12.5 h running mean was calculated.

As observed previously, pressures at the two screens in Hole 1253A are virtually identical. Both show tidal signals of the same amplitude, roughly 0.57 of the seafloor variations, as well as nearly identical average values. Data from the most recent recording period, along with data from the preceding 3 yr, are shown for the upper screen in Fig. 2a. Anomalies in the new record include a small (*c.* 0.2 kPa) negative-going one at the time of an ETS event in June 2009, and a *c.* 1 kPa a step-wise decrease in pressure at the time of the 2012 Nicoya earthquake.

The new and older records from Hole 1255A are shown in Fig. 2b, also for only one screen but for a different reason than in the case of Hole 1253A: In September 2004, a loss of seal integrity caused pressure at the deeper screen to fall from the natural over-pressured state to hydrostatic. It was speculated that that loss of pressure was the consequence of leakage past seals

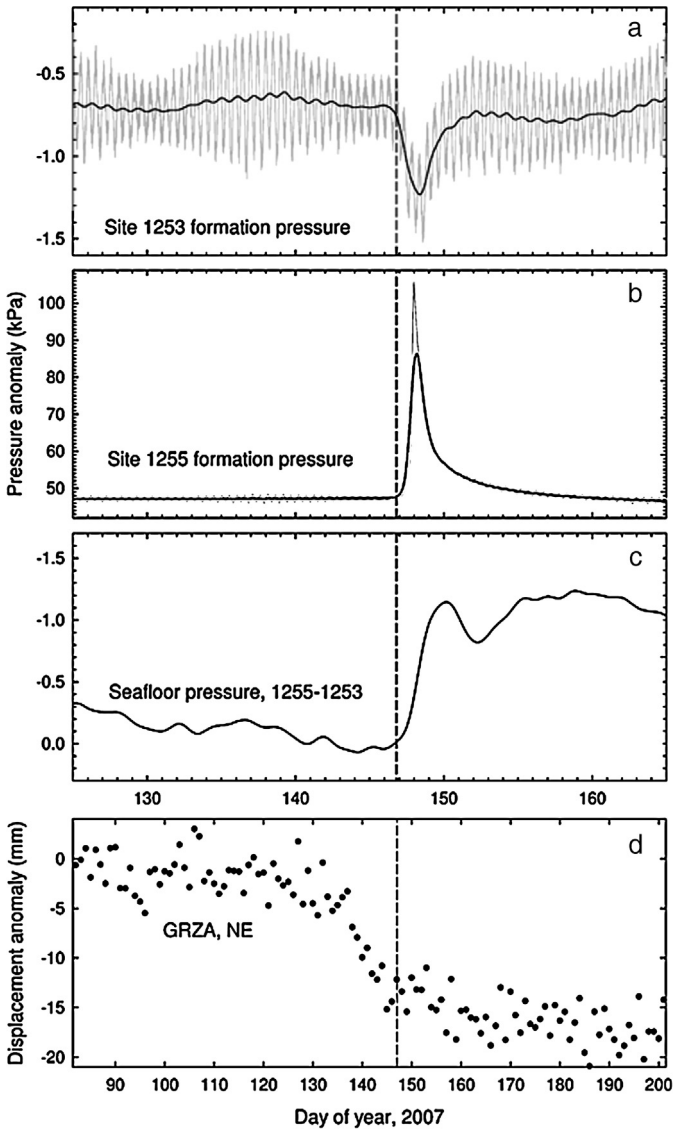

Fig. 4. Detailed views of formation pressure anomalies in Holes 1253A (a) and 1255A (b), seafloor pressure at Hole 1255A relative to Hole 1253A (c), and daily GPS data at the time of the 2007 May ETS event (d). Data are shown unfiltered and tidally filtered in (a) and (b), and filtered in (c) (see Fig. 2 caption for details). Dashed lines are shown at the time of initiation of pressure transients for reference. Note difference in time scales between (a–c) and (d).

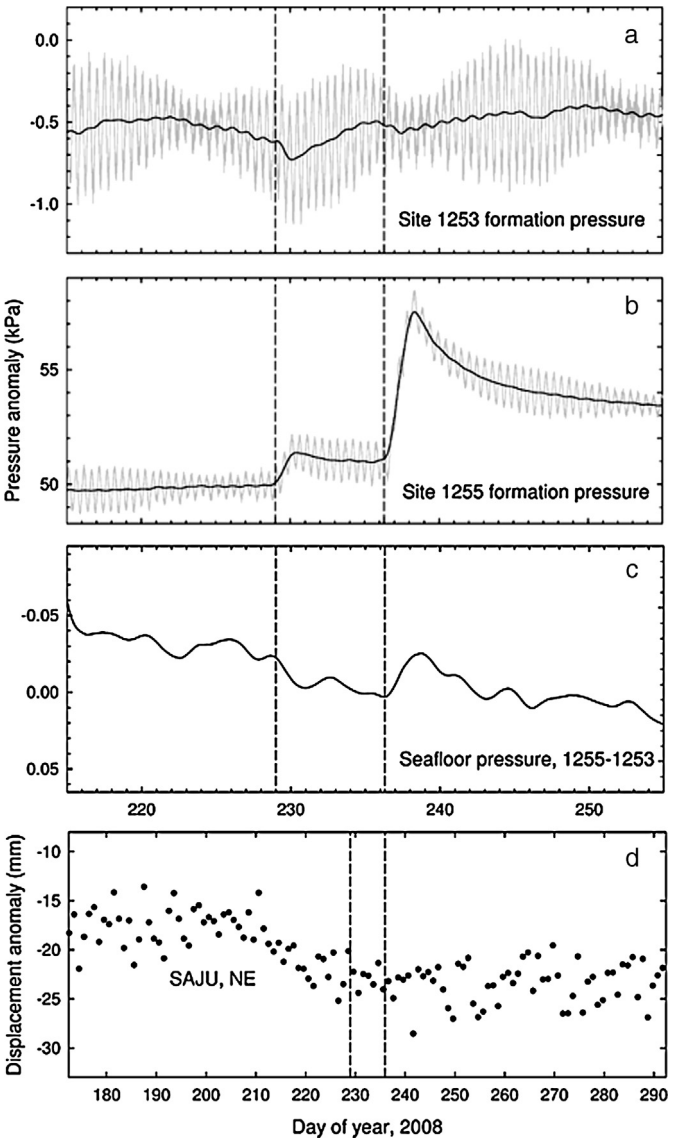

Fig. 5. Detailed views of formation pressure anomalies in Holes 1253A (a) and 1255A (b), seafloor pressure at Hole 1255A relative to Hole 1253A (c), and daily GPS data at the time of the 2008 August ETS event (d). Data are shown unfiltered and tidally filtered in (a) and (b), and filtered in (c) (see Fig. 2 caption for details). Dashed lines are shown at the time of initiation of pressure transients for reference. Note difference in time scales between (a–c) and (d).

of a geochemical fluid sampler at the bottom of the hole where the screen is located, and up the interior of the 4.5″ diameter casing string. For several years after that time, the upper screen appears to have remained hydraulically isolated, but in March 2011 pressure at this screen fell to a near-hydrostatic (+2 kPa) state (Fig. 2b). The cause of this pressure loss is also unknown, although given the short distance between this screen (at 127 mbsf) and the lower, already leaking one (at 140 mbsf), channeling along the annulus outside the casing is a possibility.

Several transients were observed prior to the seal failure, two at the time of ETS events beneath or near the Nicoya Peninsula (June 2009; October 2010), and three others that may have been precursors to the 2011 seal failure. The transient seen in 2009 is very similar to ones seen previously in 2006, 2007, and 2008. There is also a general rise in average pressure (over and above the slow secular rise seen previously and through early 2010) by about 12 kPa, beginning in March 2010 and lasting until the loss of good pressure isolation.

Unlike the complete loss of pressure at the lower screen in 2004, some hydrologic resistance appears to have been maintained after the loss of isolation of the upper screen in 2011. The formation tidal signal was attenuated relative to that at the seafloor after the loss of pressure, and the average pressure remained slightly super-hydrostatic throughout the remainder of the recording period. This partial isolation allowed a small positive transient to be resolved in mid-2011, and a step-wise and persistent change to be observed at the time of the 2012 Nicoya earthquake, when pressure dropped by roughly the same amount observed in Hole 1253A (slightly less than 1 kPa). It remained depressed for roughly 8 months after the earthquake, then increased erratically over the final 8 months of the record (Fig. 2b).

3.2. Seafloor pressures

In addition to the utility of seafloor pressure as a hydrostatic reference for interpreting formation pressures, seafloor pressure can provide information about vertical deformation. Direct use of

the records individually is limited by sensor drift and oceanographic pressure variations (Polster et al., 2009; Gennerich and Villinger, 2011). The former limits use of pressure data for determining secular signals, and the latter are significant over a broad frequency range. Tides can be removed using estimates constrained by astronomical constituents (e.g., Palowitz et al., 2002) or by simple filtering, but remaining effects (e.g., fortnightly tides, seasonal variations) can also be large relative to deformation signals. These problems have been circumvented by others through precise seafloor "surveying" of multiple benchmark sites (e.g., Chadwick et al., 2006) and use of self-calibrating instruments (Sasagawa and Zumberge, 2013).

Because the distance between the two Costa Rica observatory sites is small (920 m), many oceanographic contributions to seafloor pressure variations are common to both sites, and thus the difference in pressure between these two sites should primarily reflect differences in seafloor depth. Differences between oceanographic contributions will arise from phenomena having spatial scales equivalent to or smaller than the site spacing of (e.g., signals from infragravity waves and swell); these are unavoidable but will be small and not contribute at periods longer than about 1 min. A non-geodetic contribution to the site-to-site pressure difference will also arise from drift of the individual instrument clocks. To minimize this, the pressure record from Hole 1253A was resampled with a cubic spline interpolation routine at times equivalent to drift-corrected times of samples collected at Hole 1255A. This was done by taking clock checks done at the times of submersible visits in 2005 and 2013 at face value. A second minor time adjustment was then made to minimize the tidal residual in the difference record. Remaining residuals were removed through use of a 12.5-h running average.

The resulting history of seafloor pressure at Hole 1255A relative to that at Hole 1253A is shown in Fig. 2c. Clear signals are seen at the time of the 2009 ETS event, and at the time of and following the 2012 Nicoya earthquake. Prior to 2009, seafloor data from Hole 1253A were affected intermittently by biofouling of the sensor port. This prevented subtle signals to be seen in the long-term records, so only the last 5 yr of data are shown. Shorter time spans from the full recording history are considered in Section 4.

3.3. Coastal GPS observations

For a significant fraction of the CORK observatory recording period, GPS stations have been maintained on the Nicoya Peninsula (e.g., Outerbridge et al., 2010; Jiang et al., 2012), and have provided constraints on the timing and distribution of slow slip on the underlying subduction thrust. Observations at two of the nearest Pacific coastal sites, located directly landward of the CORK observatories (Fig. 1a) are shown in Fig. 2d. Superimposed on the northeasterly interseismic motion of the sites (a trend removed in this plot) are rapid excursions to the southwest, one in each of the years 2006–2012 spanned by these data. Associated with each of these events are transients observed at one or both of the offshore CORK sites. Several of these are discussed in the following section, along with the implications for slip across the full width of the prism.

4. Inferences about outer prism deformation and slip

4.1. Slip associated with ETS events

Detailed views of the CORK pressure signals and GPS motion at the time of the June 2009 ETS event are shown in Fig. 3. A small negative transient occurred in Hole 1253A (Fig. 3a), with the *c.* −0.3 kPa peak of the anomaly occurring at the same time as a much larger positive peak observed in Hole 1255A (Fig. 3b). The latter reached 48 kPa above the background pressure, then declined with a time constant of roughly 1 day, ultimately falling to a level 1 kPa lower than the previous background state (Fig. 2b). The seafloor data reveal a contemporaneous step-wise decrease in pressure at Hole 1255A relative to Hole 1253A of about −0.12 kPa. This change began at the time of the leading edge of the transient in Hole 1255A, and continued for roughly 2 days (Fig. 3c). Assuming that the observed uplift is a simple consequence of slip on a thrust dipping 6° (estimated from the 79 m difference between the fault depth determined by drilling at Hole 1255A and the depth of the seafloor at the prism toe, and the 750 m separation of Hole 1255A from the seafloor outcrop of the fault; see Fig. 1b; Morris et al., 2003), the inferred fault slip would be roughly 11 cm. Both the seafloor and formation pressure anomalies began near the end of the 2009 slip episode documented by the coastal GPS observations, roughly two weeks after ETS initiation (Fig. 3d).

The characteristics of these formation pressure signals are nearly identical to ones seen at the time of earlier ETS events (Davis et al., 2011), and similar to ones seen in the Nankai subduction prism at the time of very low frequency earthquake swarms (Davis et al., 2006, 2009, 2013). Those anomalies have been attributed to relaxation (dilatation) of the subducting plate and contraction of the over-riding prism caused by slow slip on the outermost part of the subduction thrust (decollement) where the holes are located (e.g., Fig. 7 of Davis et al., 2006; Screaton and Ge, 2007). The seafloor pressure signal observed at the time of the June 2009 event, which indicates uplift of the prism simultaneous with the hanging wall and footwall transients (Fig. 3c), greatly strengthens this inference regarding fault slip.

Review of formation and seafloor pressure data from Holes 1253A and 1255A at the time of earlier borehole transient events further supports this inference, and comparison of the signals recorded at the boreholes to coastal motion revealed by the GPS data shows the relative timing of signals to be consistent among events. In each case, signals at the borehole sites occurred at or near the end of the slip indicated by the coastal motion, and roughly two weeks after the beginning of the slip events (Figs. 3–5). The rate of slip estimated from the rate of uplift at the toe through the duration of these events (best defined in 2009) is roughly 5 cm/day. If slip originated at a location a few tens of km landward of the prism toe, as indicated by the location of ETS seismic activity in 2009 (S. Schwartz, pers. com., 2014) determined from the land-based seismic network described in Dixon et al. (2013), the delay in the arrival of the formation and seafloor anomalies at the prism toe would suggest an up-dip rate of propagation of the "rupture" tip of a few km/day, a rate roughly similar to one estimated by Labonte et al. (2009) on the basis of hydrologic records collected in the region at multiple prism sites prior to knowledge of ETS events.

As seen in Figs. 2c–5c, magnitudes of uplift vary, ranging from being unresolvable (limited by unaccountable oceanographic noise of roughly 0.02 kPa, or 0.2 cm water depth change) at the times of GPS-constrained slip in 2010 and 2011 (Fig. 2c), to barely resolvable in 2008 (Fig. 5c), to clearly defined at 1.2 cm in 2007 and 2009 (Figs. 4c, 3c). Amplitudes of formation pressure transients vary accordingly, with the largest occurring in 2007 and 2009 (Figs. 4a, b and 3a, b).

In the first three instances cited above (2008, 2010, and 2011 events), the inferred slip at the toe is equivalent to or less than that estimated through inversions of data from all GPS sites on the Nicoya Peninsula (Dixon et al., in press). In addition to slip down dip from the seismogenic zone, their solutions indicate slip in offshore patches typically centered 30 km off the coast with amplitudes of 2 to 3 cm. In the last two instances (2007 and 2009 events), the inferred slip at the toe is considerably larger than any of the GPS-derived estimates for slip closer to the coast. If these

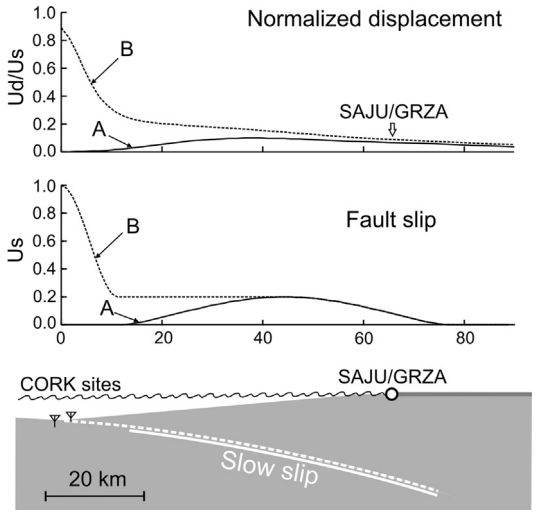

Fig. 6. Horizontal displacement at the ground/seafloor surface (upper panel) assuming two distributions of fault slip shown in center panel for a transect crossing the Nicoya Peninsula and coastal GPS sites and the prism toe CORK borehole observatories. A schematic cross section of the geometry used in the finite-element solution for displacement is shown in the lower panel. The fault slip distribution shown as a solid line is intended to be similar to a typical inversion solution for offshore ETS slip as estimated by Dixon et al. (in press). The fault slip distribution shown by the dashed line is modified to match the much larger slip estimated at the CORK sites following ETS as observed in 2007 and 2009.

estimates based on the onshore GPS and offshore uplift data are correct, they suggest that in some instances, a significant proportion of ETS slip may not reach the prism toe. At other times it may, and in some cases (e.g., 2007 and 2009) "deficits" may be made up for, with greater amounts of slip taking place beneath the outermost part of the prism than the inner.

Given that slip is unquestionably patchy and that the spatial distribution of observations is poor, it is impossible to draw quantitatively accurate conclusions about the details of offshore deformation and slip. The location of the offshore borehole observatories is singular, and the ability for onshore GPS observations to constrain deformation offshore falls rapidly with distance from the coast. This insensitivity is illustrated in Fig. 6, where the cross-strike ground-surface displacement is shown for two contrasting cases of fault slip, one following a distribution similar to ones estimated from GPS inversions, and one with slip extending to the trench and growing by a factor of five over the seaward-most 10 km. This simple two-dimensional conceptualization is not intended to be "realistic"; it is intended only to show that the occasional presence of large slip near the trench, as suggested in some cases by the offshore uplift data, is not precluded by the onshore GPS displacement observations. Such a spatially variable pattern of elastic storage and slow-slip release must remain speculative, however, until additional offshore observation can be made.

4.2. The 2012 Nicoya earthquake

Detailed views of the formation and seafloor pressure anomalies at the time of the 2012 Nicoya Peninsula earthquake are shown in Fig. 7. Unlike the "co-seismic" strain at the time of ETS events (i.e., the far-field strain resulting from the near-coastal ETS slip itself) which is much too small to be detected at the borehole sites (e.g., Fig. 4a of Davis et al., 2011), the co-seismic strain caused by the 2012 Nicoya earthquake is well resolved in formation pressure (Fig. 7a, b). Negative steps are seen at both sites, indicating dilatation. The magnitude (roughly −0.5 kPa in both holes) suggests a volumetric strain of roughly 0.1×10^{-6}, assuming properties estimated previously (e.g., Fig. 6 of Davis et al., 2009). At first glance the sign seems counterintuitive; a simple dislocation model for the

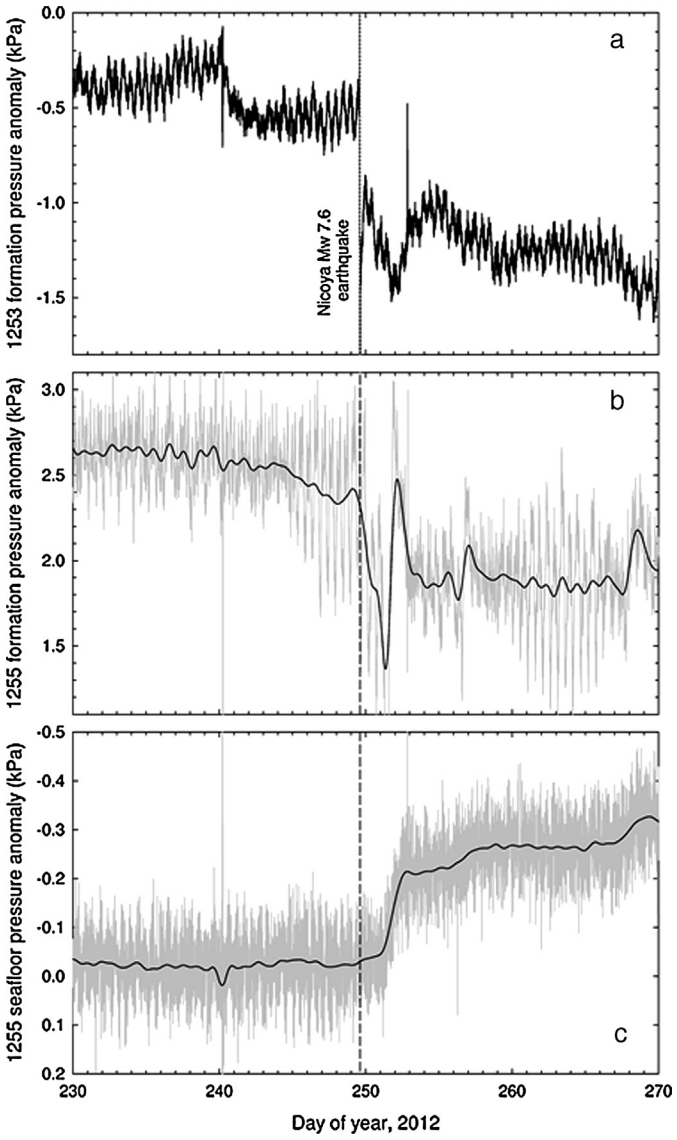

Fig. 7. Detailed view of formation pressure anomalies in Holes 1253A (a) and 1255A (b), and seafloor pressure at Hole 1255A relative to Hole 1253A (c) at the time of the 2012 Nicoya earthquake. Unfiltered data are shown in (a), and both filtered (black) and unfiltered (grey) data are shown in (b) and (c). Small amplitudes of anomalies in Hole 1255A (b) are likely to be the result of leakage past compromised CORK seals.

earthquake would predict volumetric contraction at the location of both boreholes (e.g., Fig. 4a of Davis et al., 2011, and Fig. 9 below). Two possible explanations for the sign of the observed anomalies are discussed later in this section.

The detailed view of the seafloor pressure anomaly (Fig. 7c) resolves no co-seismic signal, but a post-seismic anomaly is observed that is very much like those shown in Figs. 3–5 associated with the 2007, 2008, and 2009 ETS events. Pressure at the prism toe site begins to decrease relative to the incoming plate site roughly two days after the earthquake, and continues to change by −0.17 kPa, equivalent to 1.7 cm of uplift, over the course of the next two days. If this reflects thrust motion along the dipping decollement, it suggests a slip of 16 cm.

The detailed views of the formation pressure records also show post-seismic signals that are concurrent with the first indication of uplift in the seafloor record, specifically a negative-going anomaly at Hole 1253A (Fig. 7a) and a positive impulsive anomaly at Hole 1255A (Fig. 7b). A view over a longer period of time (Fig. 8) reveals several correlated anomalies like this, with episodic step-wise

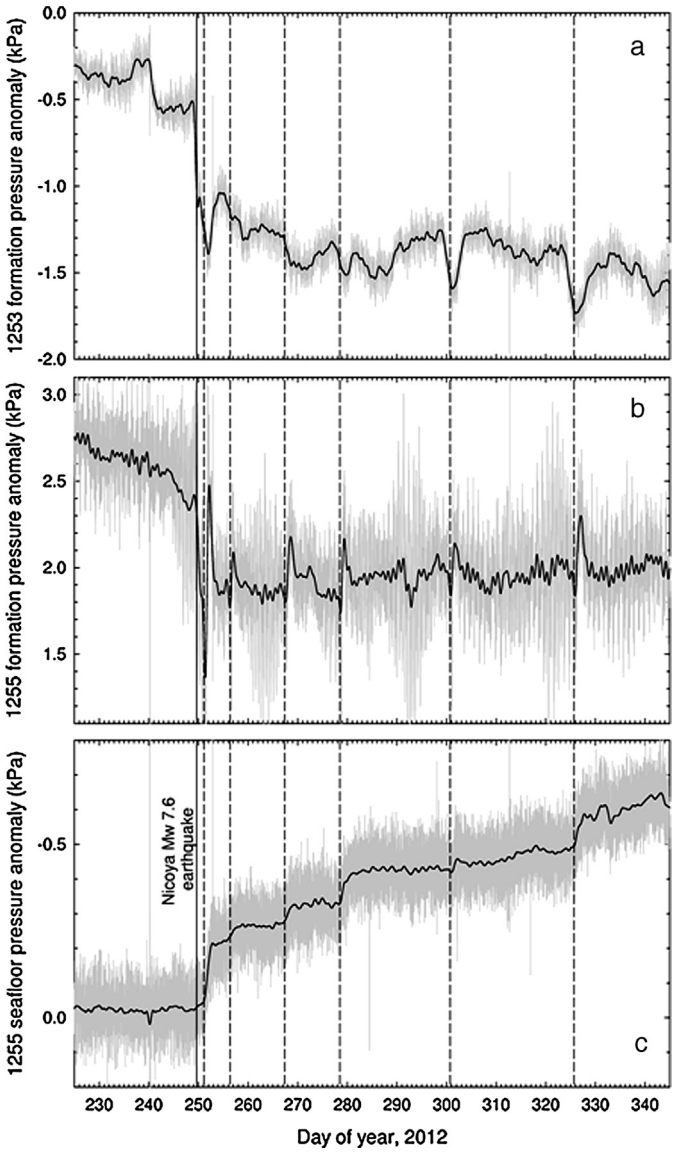

Fig. 8. Expanded (150-day) view of formation pressure anomalies in Holes 1253A (a) and 1255A (b), and seafloor pressure at Hole 1255A relative to Hole 1253A (c), including the first 100 days after the 2012 Nicoya earthquake. Filtered (black) and unfiltered (grey) data are shown in all plots.

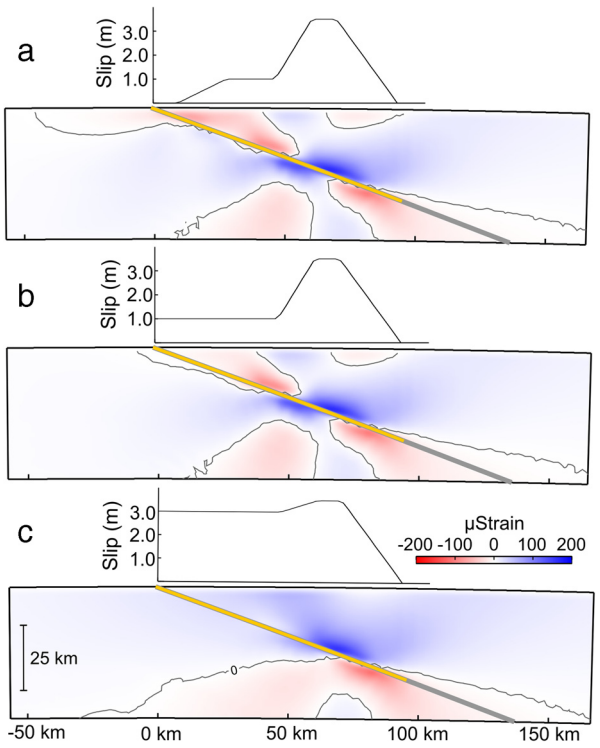

Fig. 9. Volumetric strain field for a uniform-properties domain calculated with a finite-element elastic model assuming slip on a fault as constrained by seismic data (Yue et al., 2013, Fig. 5) (a), and slip modified to extend to the prism toe (b, c) (to simulate low-stress shear beneath or within the outermost prism following the schematic of Fig. 10). The two cases of extended slip shown in (b) and (c) bracket the threshold amount of effective slip required to cause dilatation at the prism toe. The model is highly simplified (e.g., it is two-dimensional, whereas the actual co-seismic slip distribution was limited in the along-strike direction), and is not intended to be quantitatively correct. Its purpose is only to show that a large amount of deformation must be absorbed at the prism toe with little stress to yield the sign of co-seismic deformation observed at the CORK sites.

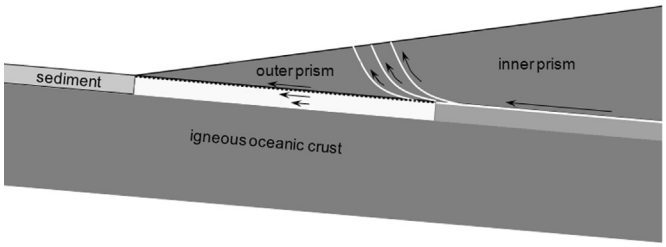

Fig. 10. Interpretive sketch showing hypothetical means by which the outer subduction prism might be decoupled from the inner prism, either via distributed shear along weak splay faults, or via low-stress shear of low-modulus sediment beneath the outer prism (depicted by light grey layer).

uplift occurring concurrently with positive impulsive anomalies at Hole 1255A and small negative ones at Hole 1253A, each looking very much like the anomalies following the 2009 and other ETS events. None of the post-seismic anomalies is associated with aftershocks in the Nicoya earthquake epicentral area (J. Walter, pers. com.). They appear to be spontaneous, although the possibility that they originate from undetected ETS-like afterslip in the epicentral area cannot be ruled out.

While the direct association of uplift with formation fluid pressure transients removes doubt about the existence of discrete slow slip in the outermost prism following ETS events and the 2012 earthquake, the observed *co-seismic* formation pressure transients at the time of the Nicoya earthquake present an apparent paradox: Co-seismic step-wise decreases in formation pressure in both the prism toe (Hole 1255A) and the incoming plate (Hole 1253A) suggest dilatational strain, whereas contractional strain is expected on the basis of a fault dislocation model in a medium with uniform properties (Fig. 9a). A schematic illustration of two hypothetical modes of deformation that could account for the sign of the observed co-seismic pressure transients is shown in Fig. 10. One involves throw on splay faults or fractures located between the prism toe and the seaward limit of seismogenic slip (e.g., Silver, 2000), in a part of the prism that might be characterized by low fault friction (Ikari et al., 2009) or low effective shear modulus and thus that could easily absorb slip. The other includes a compliant sediment layer sandwiched between the top of the down-going oceanic crust and the overriding prism. In the case of Costa Rica, such a layer is likely to be present. Much or all of the 400–500 m thickness of the section arriving at the trench is inferred to be carried to great depth (Silver, 2000; von Huene and Scholl, 1991), and at locations not far landward of the prism toe its physical properties are likely to contrast greatly with the properties of material above and below. Immediately following subduction, the initially high porosity of the incoming section will decrease as the load imposed by the upper

plate increases, but to the degree that compaction is impeded by the inability of pore water to escape (under the control of permeability, the rate of loading, and the hydrologic drainage path length), pore fluid pressure will rise (e.g., Screaton et al., 1990, 2002; Bekins and Dreiss, 1992; Spinelli and Underwood, 2004; Saffer and Bekins, 2006; Saffer, 2003, 2007), causing the sediment to become even more compliant than it already is (e.g., Tsuji et al., 2011). This effect will dominate until fluid flux, compaction, and increasing temperature promote significant compaction and diagenesis, with attendant stiffening and strengthening to the point of allowing seismogenesis (e.g., Hyndman and Wang, 1995; Moore and Saffer, 2001; Marone and Saffer, 2007; Lay et al., 2012).

Between the updip limit of seismogenic slip and the toe of the prism, the presence of highly compliant material (in either of the scenarios sketched in Fig. 10) may profoundly influence the distribution of strain at the time of a subduction earthquake. It may effectively decouple the hanging wall and foot wall of the thrust, cause stresses in the outer part of the prism to be much lower than those generated in higher-modulus material, and cause the far-field co-seismic strain to be more like that produced when a large amount of fault slip reaches the seafloor (Fig. 9c) than that produced by a modest amount of slip (Fig. 9b) or by slip limited to the area responsible for seismogenesis (Fig. 9a). The small shear stress that remains stored in compliant volumes would be available to drive slow post-seismic slip along the decollement (i.e., the "mudquakes" of Fig. 8), the plane of greatest weakness.

Although speculative, such a model does provide a plausible explanation for the observed co-seismic dilatation at both CORK observatory sites, and subsequent episodic and chronic slip along the decollement. The presence of low-modulus material has been inferred previously on the basis of the depth-dependent character of subduction-thrust seismic radiation (Bilek and Lay, 1999), and from anomalous outer-prism seismic velocities (Tobin and Saffer, 2009; Park et al., 2010; Tsuji et al., 2011). Splay faults seaward of the seismogenic zone are observed here and elsewhere (Silver, 2000; Moore et al., 2007; Bangs et al., 2009; Kimura et al., 2011). And sediments are subducted at most subduction zones (von Huene and Scholl, 1991). At Nankai the subduction prism is known to host very low stress-drop earthquakes (Ito and Obara, 2006; Kitajima and Saffer, 2012), and the decollement is marked by a clear reversal in the sediment porosity-depth trend, indicating that the under-thrust section is under-consolidated, almost certainly overpressured, and probably characterized by a low shear modulus (Taira et al., 1991; Hyndman et al., 1993; Tobin and Saffer, 2009; Tsuji et al., 2011).

Understanding the role that low-strength splay faults and low-modulus material within or beneath the outer prism may play in elastic and permanent prism deformation has important implications for subduction thrust seismogenesis and tsunamigenesis. For example, low modulus material may be important in limiting the updip extent of seismogenesis (as an important or even dominating complement to the velocity-strengthening behavior of the decollement). If shear in a compliant layer absorbs much of the coseismic strain updip of the seismogenic zone, uplift at the prism toe might be minor, eliminating the outermost part of the prism as a source for tsunamigenesis. Significant uplift may occur only when there is slip along the decollement itself. In the example presented here, this did occur, but much too slowly to be seismogenic or tsunamigenic. In cases like the devastating 2012 Tohoku earthquake (Fujiwara et al., 2011; Kimura et al., 2012; Kodaira et al., 2012), the 1992 tsunami earthquake off Nicaragua (Satake, 1994), and the 2010 Mentawai tsunami earthquake (Newman et al., 2011), slip beneath the outermost prism must have been relatively rapid. Just what causes such contrasting behavior remains unresolved.

5. Summary and conclusions

Five-year records of seafloor temperature and formation- and seafloor-pressure observations, collected in December 2013 from ODP Holes 1253A and 1255A off Costa Rica, roughly double previous time-series data spanning from late 2002 through 2008, and include signals associated with an ETS event in June 2009, and with the September 2012 magnitude 7.6 thrust earthquake beneath Nicoya Peninsula.

Post-seismic signals beginning 2 days after the 2012 earthquake include a series of transient anomalies, each with simultaneous stepwise decreases in seafloor pressure at the prism toe (indicating uplift), positive impulsive pore-fluid pressure transients within the prism (indicating contraction), and negative impulsive transients within the subducting plate (indicating dilatation). The formation pressure anomalies are directly analogous to ones seen at the times of ETS events in 2007, 2008, and 2009, and similar to signals seen at the Nankai subduction zone (Davis et al., 2006, 2009, 2013). The new observations presented here showing uplift at the prism toe at the times of most of the formation-pressure transients confirm that the formation anomalies must be the consequence of slow but discrete slip events along the decollement (thrust "mudquakes") as inferred previously by Davis et al. (2006) and Screaton and Ge (2007). This strengthened inference can probably be extended retrospectively to the interpretation of transient tremor-like seismic "noise" and seafloor fluid-flux anomalies observed previously off Costa Rica (Brown et al., 2005; Labonte et al., 2009). The timing of the seafloor- and formation-pressure transients suggests that slip propagates updip from the zone of earthquake and ETS genesis (a few tens of km landward of the prism toe) at rates of the order of a few km/day. The *c.* 2-day durations of uplift-inferred slip suggests slip rates of roughly 5 cm/day. Neither the rate of propagation nor the rate of slip is anywhere close to being seismogenic or tsunamigenic. Just what constrains the rates of propagation and slip remains for now without explanation, but some interplay among shear strain, porosity change, and pore-fluid pressure is likely to be involved.

Over the 1.3 yr of recording after the Nicoya earthquake, the accumulated uplift totaled 8 cm (Fig. 2c), with roughly half taking place in an irregular manner with no clearly related formation pressure variations (Fig. 2a, b). If the total uplift reflects slip on a fault dipping at 6°, the amount of slip would be 76 cm. This is a fraction of the maximum estimated seismogenic fault slip (over 3 m), but commensurate with the seismogenic slip estimated in the more distal parts of the earthquake rupture area (Yue et al., 2013). In contrast, inferred slip observed in 2007 and 2008 beneath the prism toe was greater than the preceding ETS slip further landward as estimated by Dixon et al. (in press). This shows the temporal and spatial distribution of elastic storage and slip in the outer part of this subduction zone to be heterogeneous. Such complexity cannot be resolved by onshore observations alone.

While some of the implications of the co-seismic formation transients at the time of the 2012 Nicoya earthquake are speculative, many things are clear. Our observations show that relatively simple methods can be employed to track both seismic and inter-seismic deformation offshore. Seafloor pressure monitoring is simple and inexpensive, yet can provide unique constraints on prism deformation and fault slip. Borehole observatories are expensive to establish, but if properly located (guided by the knowledge gained from the early deployments that were sited with considerable serendipity, and by now-known locations of frequent episodic deformation) they can add important complementary information. Future observations like these, made over appropriate cross- and along-strike scales at this and other subduction zones, will provide valuable insight into inter-seismic and co-seismic deformation, seismogenesis, and tsunamigenesis.

Acknowledgements

Data were recovered via the remotely operated vehicle Jason on RV Atlantis during a cruise funded by the U.S. National Science Foundation. Bob Meldrum and Bob Macdonald have provided technical expertise throughout the lifetime of this Ocean Drilling Program CORK installation and monitoring project. Credit for the long and reliable lifetime of the instruments must also be given to suppliers of components, including Richard Brancker Research, Ltd., Paroscientific, Inc., SeaCon/Brantner and Associates, Inc., Mecco, Inc., and Tadiran, Ltd. for data loggers, pressure sensors, cables and connectors, and batteries, respectively. Funding for instruments and site visits has been provided through U.S. National Science Foundation Grants OCE-25145 and -1130146. The finite element code used for the dislocation modeling was developed by Jiangheng He. Helpful comments were provided by Susan Schwartz and an anonymous reviewer.

References

Bangs, N.L.B., Moore, G.F., Gulick, S.P.S., Pangborn, E.M., Tobin, H.J., Kuramoto, S., Taira, A., 2009. Broad, weak regions of the Nankai Megathrust and implications for shallow coseismic slip. Earth Planet. Sci. Lett. 284, 44–49.

Bekins, B.A., Dreiss, S.J., 1992. A simplified analysis of parameters controlling dewatering in accretionary prisms. Earth Planet. Sci. Lett. 109, 275–287.

Bilek, S., Lay, T., 1999. Rigidity variations with depth along interpolate megathrust faults in subduction zones. Nature 400, 443–446.

Brown, K.M., Tryon, M.D., DeShon, H.R., Dorman, L.M., Schartz, S.Y., 2005. Correlated transient fluid pulsing and seismic tremor in the Costa Rica subduction zone. Earth Planet. Sci. Lett. 238, 189–203.

Chadwick, W.W., Nooner, S.L., Zumberge, M.A., Embley, R.W., Fox, C.G., 2006. Vertical deformation monitoring at Axial Seamount since its 1998 eruption using deep-sea pressure sensors. J. Volcanol. Geotherm. Res. 150, 313–327.

Davis, E.E., Villinger, H., 2006. Transient formation fluid pressures and temperatures in the Costa Rica forearc prism and subducting oceanic basement: CORK monitoring at ODP Sites 1253 and 1255. Earth Planet. Sci. Lett. 245, 232–244.

Davis, E.E., Becker, K., Wang, K., Obara, K., Ito, Y., Kinoshita, M., 2006. A discrete episode of seismic and aseismic deformation of the Nankai subduction zone accretionary prism and incoming Philippine Sea plate. Earth Planet. Sci. Lett. 242, 73–84.

Davis, E.E., Becker, K., Wang, K., Kinoshita, M., 2009. Co-seismic and post-seismic pore-fluid pressure changes in the Philippine Sea plate and Nankai decollement in response to a seismogenic strain event off Kii Peninsula, Japan. Earth Planets Space 61, 649–657.

Davis, E.E., Heesemann, M., Wang, K., 2011. Evidence for episodic aseismic slip across the subduction seismogenic zone off Costa Rica: CORK borehole pressure observations at the subduction prism toe. Earth Planet. Sci. Lett. 306, 299–305.

Davis, E.E., Kinoshita, M., Wang, K., Asano, Y., Ito, Y., Becker, K., 2013. Episodic deformation and inferred slow slip at the Nankai subduction zone during the first decade of CORK borehole pressure and VLFE monitoring. Earth Planet. Sci. Lett. 368, 110–118.

Dixon, T., Schwartz, S., Protti, M., Gonzalez, V., Newman, A., Marshall, J., Spotila, J., 2013. Eos 94, 17–28.

Dixon, T., Jiang, Y., Malservisi, R., McCaffrey, R., Voss, N., Protti, M., Gonzalez, V., in press. Earthquake and tsunami forecasts: relation of slow slip events to subsequent earthquake rupture. Proc. Natl. Acad. Sci. http://dx.doi.org/10.1073/pnas.1412299111.

Fujiwara, T., Kodaira, S., No, T., Kaiho, Y., Takahashi, N., Kaneda, Y., 2011. The 2011 Tohoku-Oki earthquake: displacement reaching the trench axis. Science 334, 1240.

Gennerich, H.-H., Villinger, H., 2011. Deciphering the ocean bottom pressure variation in the Logatchev Hydrothermal Field at the eastern flank of the Mid-Atlantic Ridge. Geochem. Geophys. Geosyst. 12, Q0AE03. http://dx.doi.org/10.1029/2010GC003441.

Hill, E.M., Borrero, J.C., Huang, Z., et al., 2012. The 2010 Mw 7.8 Mentawai earthquake: very shallow source of a rare tsunami earthquake determined from tsunami field survey and near-field GPS data. J. Geophys. Res. 117, B06402. http://dx.doi.org/10.1029/2012JB009159.

Hirose, H., Asano, Y., Obara, K., Kimura, T., Matsuzawa, T., Tanaka, S., Maeda, T., 2010. Slow earthquakes linked along dip in the Nankai subduction zone. Science 330, 1502.

Hsu, Y.-J., Simons, M., Avouac, J.-P., Galetzka, J., Sieh, K., Chlieh, M., Natawidjaja, D., Prawirodirdjo, L., Bock, Y., 2006. Frictional afterslip following the 2005 Nias-Simeulue earthquake, Sumatra. Science 312, 1921–1926.

Hyndman, R.D., Wang, K., 1995. The rupture area of Cascadia great earthquakes from current deformation and the thermal regime. J. Geophys. Res. 100, 22133–22154.

Hyndman, R.D., Moore, G.F., Moran, K., 1993. Velocity, porosity, and pore-fluid loss from the Nankai subduction zone accretionary prism. Proc. Ocean Drill. Program Sci. Results 131, 211–219.

Iinuma, T., Hino, R., Kido, M., Inazu, D., Osada, Y., Ito, Y., Ohzono, M., Tsushima, H., Suzuki, S., Fujimoto, H., Miura, S., 2012. Coseismic slip distribution of the 2011 off the Pacific Coast of Tohoku Earthquake (M9.0) refined by means of seafloor geodetic data. J. Geophys. Res. 117, B07409. http://dx.doi.org/10.1029/2012JB009186.

Ikari, M.J., Saffer, D.M., Marone, C., 2009. Frictional and hydrologic properties of a major splay fault system, Nankai subduction zone. Geophys. Res. Lett. 36, L20313.

Ito, Y., Obara, K., 2006. Very low frequency earthquakes within accretionary prisms are very low stress-drop earthquakes. Geophys. Res. Lett. 33, L09302.

Jannasch, H.W., Davis, E.E., Kastner, M., Morris, J.D., Pettigrew, T.L., Plant, J.N., Solomon, E.A., Villinger, H.W., Wheat, C.G., 2003. CORK II: long-term monitoring of fluid chemistry, fluxes, and hydrology in instrumented boreholes at the Costa Rica subduction zone. In: Morris, J.D., Villinger, H.W., Klaus, A. (Eds.), Proc. ODP, Init. Repts., vol. 205.

Japan Coast Guard and Tohoku University, 2013. Seafloor movements observed by seafloor geodetic observations after the 2011 off the Pacific coast of Tohoku Earthquake. In: Report of Coordinating Committee of Earthquake Prediction, vol. 90, pp. 3–4. http://cais.gsi.go.jp/YOCHIREN/report/kaihou90/03_04.pdf.

Jiang, Y., Wdowinski, S., Dixon, T.H., Hackl, M., Protti, M., Gonzalez, V., 2012. Slow slip events in Costa Rica detected by continuous GPS observations, 2002–2011. Geochem. Geophys. Geosyst. 13, Q04006. http://dx.doi.org/10.1029/2012GC004058.

Kido, M., Osada, Y., Fujimoto, H., Hino, R., Ito, Y., 2011. Trench-normal variation in observed seafloor displacements associated with the 2011 Tohoku-Oki earthquake. Geophys. Res. Lett. 38, L24303.

Kimura, G., Moore, G.F., Strasser, M., Screaton, E., Curewitz, D., Streiff, C., Tobin, H., 2011. Spatial and temporal evolution of the megasplay fault in the Nankai Trough. Geochem. Geophys. Geosyst. 12, Q0A008.

Kimura, G., Hina, S., Hamada, Y., Kameda, J., Tsuji, T., Kinoshita, M., Yamaguchi, A., 2012. Runaway slip to the trench due to rupture of highly pressurized megathrust beneath the middle trench slope: the tsunamigenesis of the 2011 Tohoku earthquake off the east coast of northern Japan. Earth Planet. Sci. Lett. 339–340, 32–45.

Kitajima, H., Saffer, D.M., 2012. Elevated pore pressure and anomalously low stress in regions of low frequency earthquakes along the Nankai Trough subduction megathrust. Geophys. Res. Lett. 39, L23301. http://dx.doi.org/10.1029/2012GL053793.

Kodaira, S., No, T., Nakamura, Y., Fujiwara, T., Kaiho, Y., Miura, S., Takahashi, N., Kaneda, Y., Taira, A., 2012. Coseismic fault rupture at the trench axis during the 2011 Tohoku-oki earthquake. Nat. Geosci. 5, 646–650.

Labonte, A.L., Brown, K.M., Fialko, Y., 2009. Hydrologic detection and finite element modeling of a slow slip event in the Costa Rica prism toe. J. Geophys. Res. 114, B00A02.

Lay, T., Kanamori, H., Ammon, C.J., Koper, K.D., Hutko, A.R., Ye, L., Yue, H., Rushing, T.M., 2012. Depth-varying rupture properties of subduction zone megathrust faults. J. Geophys. Res. 117, B04311.

Maeda, T., Furumura, T., Sakai, S., Shinohara, M., 2011. Significant tsunami observed at ocean-bottom pressure gauges during the 2001 off the Pacific coast of Tohoku earthquake. Earth Planets Space 63, 803–808.

Marone, C., Saffer, D., 2007. Fault friction and the upper transition from seismic to aseismic faulting. In: Dixon, T.H., Moore, J.C. (Eds.), The Seismogenic Zone of Subduction Thrust Faults. Columbia University Press, New York, pp. 346–369.

Moore, J.C., Saffer, D.M., 2001. Updip limit of the seismogenic zone beneath the accretionary prism of southwest Japan: an effect of diagenetic to low-grade metamorphic processes and increasing effective stress. Geology 29, 183–238.

Moore, G.F., Bangs, N.L., Taira, A., Kuramoto, S., Pangborn, E., Tobin, H.J., 2007. Three-dimensional splay fault geometry and implications for tsunami generation. Science 318, 1128–1131.

Morris, J.D., Villinger, H., Klaus, A., Shipboard Scientific Party, 2003. Proc. Ocean Drilling Program, Init. Repts., vol. 205. Ocean Drilling Program, College Station, TX. 611 pp.

Newman, A.V., Hayes, G., Wei, Y., Convers, J., 2011. The 25 October 2010 Mentawai tsunami earthquake, from real-time discriminants, finite fault rupture, and tsunami excitation. Geophys. Res. Lett. 38, L05302. http://dx.doi.org/10.1029/2010GL046498.

Obara, K., Ito, Y., 2005. Very low frequency earthquakes excited by the 2004 off the Kii peninsula earthquakes: a dynamic deformation process in the large accretionary prism. Earth Planets Space 57, 321–326.

Outerbridge, K.C., Dixon, T.H., Schwartz, S.Y., Walter, J.I., Protti, M., Gonzalez, V., Biggs, J., Thorwart, M., Rabbel, W., 2010. A tremor and slip event on the Cocos–Caribbean subduction zone as measured by a global positioning system (GPS) and seismic network on the Nicoya Peninsula, Costa Rica. J. Geophys. Res. 115, B10408. http://dx.doi.org/10.1029/2009JB006845.

Palowitz, R., Beardsley, B., Lentz, S., 2002. Classical tidal harmonic analysis including error estimates in MATLAB using T_TIDE. Comput. Geosci. 28, 929–937.

Park, J.-O., Fujie, G., Wijerathne, L., Hori, T., Kodaira, S., Fukao, Y., Moore, G., Bangs, N., Kuramoto, S., Taira, A., 2010. A low-velocity zone with weak reflectivity along the Nankai subduction zone. Geology 38, 283–286. http://dx.doi.org/10.1130/G30205.1.

Polster, A., Fabian, M., Villinger, H., 2009. Effective resolution and drift of Paroscientific pressure sensors derived from long-term seafloor measurements. Geochem. Geophys. Geosyst. 10, Q08008. http://dx.doi.org/10.1029/2009GC002532.

Protti, M., et al., 2004. A creep event on the shallow interface of the Nicoya Peninsula, Costa Rica seismogenic zone. In: AGU Fall Meeting Abstracts, 85, D7.

Protti, M., Gonzalez, V., Newman, A.V., et al., 2013. Nicoya earthquake rupture anticipated by geodetic measurement of the locked plate interface. Nat. Geosci.. http://dx.doi.org/10.1038/ngeo2038.

Saffer, D.M., 2003. Pore pressure development and progressive dewatering in underthrust sediments at the Costa Rican subduction margin: comparison with northern Barbados and Nankai. J. Geophys. Res. 108 (B5), 2261. http://dx.doi.org/10.1029/2002JB001787.

Saffer, D.M., 2007. Pore pressure within underthrust sediment in subduction zones. In: Dixon, T.H., Moore, J.C. (Eds.), The Seismogenic Zone of Subduction Thrust Faults. Columbia University Press, New York, pp. 171–209.

Saffer, D.M., Bekins, B.A., 2006. An evaluation of factors influencing pore pressure in accretionary complexes: implications for taper angle and wedge mechanics. J. Geophys. Res. 111, B04101. http://dx.doi.org/10.1029/2005JB003990.

Sasagawa, G., Zumberge, M.A., 2013. A self-calibrating pressure recorder for detecting seafloor height change. IEEE J. Ocean. Eng. 38, 447–454. http://dx.doi.org/10.1109/joe.2012.2233312.

Satake, K., 1994. Mechanism of the 1992 Nicaragua tsunami earthquake. Geophys. Res. Lett. 21, 2519–2522.

Screaton, E., Ge, S., 2007. Modeling of the effects of propagating thrust slip on pore pressures and implications for monitoring. Earth Planet. Sci. Lett. 258, 454–464.

Screaton, E.J., Wurthritch, D.R., Dreiss, S.J., 1990. Permeabilities, fluid pressures, and flow rates in the Barbados ridge complex. J. Geophys. Res. 95, 8997–9007.

Screaton, E.J., Saffer, D.M., Henry, P., Hunze, S., Leg 190 Shipboard Scientific Party, 2002. Porosity loss within underthrust sediment of the Nankai accretionary complex: implications for overpressures. Geology 30, 19–22.

Silver, E.A., 2000. Leg 170: synthesis of fluid-structural relationships of the Pacific margin of Costa Rica. In: Silver, E.A., Kimura, G., Shipley, T.H. (Eds.), Proc. ODP, Sci. Results, vol. 170, pp. 1–11.

Solomon, E.A., Kastner, M., Wheat, C.G., Jannasch, H., Robertson, G., Davis, E.E., Morris, J.D., 2009. Long-term hydrogeochemical records in the oceanic basement and forearc prism at the Costa Rica subduction zone. Earth Planet. Sci. Lett. 282, 240–251.

Spinelli, G.A., Underwood, M.B., 2004. Character of sediments entering the Costa Rica subduction zone: implications for partitioning of water along the plate interface. Isl. Arc 13, 432–451.

Sun, T., Wang, K., Iinuma, T., Hino, R., He, J., Fujimoto, H., Kido, M., Osada, Y., Miura, S., Ohta, Y., Hu, Y., 2014. Prevalence of viscoelastic relaxation after the 2011 Tohoku-oki earthquake. Nature 514, 84–87. http://dx.doi.org/10.1038/nature13778.

Taira, A., Hill, I.A., Firth, J.V., Shipboard Scientific Party, 1991. Proc. ODP Init. Rept., vol. 131. Ocean Drilling Program, College Station, TX. 434 pp.

Thomson, R.E., Davis, E.E., Heesemann, M., Villinger, H., 2010. Observations of long-duration episodic bottom currents in the Middle America Trench: evidence for tidally initiated turbidity flows. J. Geophys. Res. 115, C10020. http://dx.doi.org/10.1029/2010JC006166.

Tobin, H., Saffer, D., 2009. Elevated fluid pressure and extreme mechanical weakness of a plate boundary thrust, Nankai Trough subduction zone. Geology 37, 679–682.

Tsuji, T., et al., 2011. V_p/V_s ratio and shear-waves splitting in the Nankai Trough seismogenic zone: insights into effective stress, pore pressure and sediment consolidation. Geophysics 76 (3), WA71–WA82.

Von Huene, R., Scholl, D.W., 1991. Observations at convergent margins concerning sediment subduction, subduction erosion, and the growth of continental crust. Rev. Geophys. 29, 279–316.

Walter, J.I., Schwartz, S.Y., Protti, J.M., Gonzalez, V., 2011. Persistent tremor within the northern Costa Rica seismogenic zone. Geophys. Res. Lett. 38, L01307. http://dx.doi.org/10.1029/2010GL045586.

Walter, J.I., Schwartz, S.Y., Protti, M., Gonzalez, V., 2013. The synchronous occurrence of shallow tremor and very low frequency earthquakes offshore of the Nicoya Peninsula, Costa Rica. Geophys. Res. Lett. 40, 1517–1522.

Yue, H., Lay, T., Schwartz, S.Y., Rivera, L., Protti, M., Dixon, T.H., Owen, S., Newman, A.V., 2013. The 5 September 2012 Nicoya, Costa Rica Mw 7.6 earthquake rupture process from joint inversion of high-rate GPS, strong-motion, and teleseismic P wave data and its relationship to adjacent plate boundary interface properties. J. Geophys. Res. 118, 5453–5466. http://dx.doi.org/10.1002/jgrb.50379.